Control of the Anomalous Hall Effect by Doping in $Eu_{1-x}La_xTiO_3$ Thin Films

K. S. Takahashi,[1] M. Onoda,[2] M. Kawasaki,[1,3] N. Nagaosa,[1,4] and Y. Tokura[1,4,5]

[1]*Cross-correlated Materials Research Group (CMRG), Advanced Science Institute, RIKEN, Wako 351-0198, Japan*
[2]*Department of Electrical and Electronic Engineering, Akita University, Akita 010-8502, Japan*
[3]*WPI Advanced Institute for Materials Research and Institute for Materials Research, Tohoku University, Sendai 980-8577, Japan*
[4]*Department of Applied Physics, University of Tokyo, Tokyo 113-8656, Japan*
[5]*Multiferroics Project, ERATO, Japan Science and Technology Agency (JST), Tokyo 113-8656, Japan*

(Received 24 December 2008; published 31 July 2009)

The anomalous Hall effect (AHE) has been studied for epitaxial films of $Eu_{1-x}La_xTiO_3$, in which band filling can be controlled by doping x without undesired changes in magnetization. This system has a simple band structure near the conduction band bottom, which makes it possible to design the AHE. As expected, the anomalous Hall resistivity shows a nonmonotonic change as a function of the carrier density accompanied with the sign reversal around $n = 2.4 \times 10^{20}$ cm^{-3}. This opens a possibility to control the AHE by devising the material, structure, and doping level.

DOI: 10.1103/PhysRevLett.103.057204 PACS numbers: 75.47.−m, 72.15.−v, 75.70.−i

Spin related transport phenomena attract a growing interest because of recent progress in spintronics research [1–3]. It has been known that the spontaneous magnetization contributes to the Hall resistivity in ferromagnets. This component is well known as the anomalous Hall effect (AHE), in addition to the normal component that is proportional to the magnetic field. The origin of the AHE has been a subject of condensed-matter physics for many years, which is also of renewed interest in spintronics applications. On the basis of the band picture, Karplus and Luttinger proposed that the AHE is attributed to anomalous velocity induced by spin-orbit interaction [4]. On the other hand, what most theories postulated was that the scattering modified by the spin-orbit interaction generates the AHE, i.e., skew scattering [5] and the side jump mechanism [6], termed as the extrinsic mechanism. Recently, theories based on the concept of Berry phase have been proposed as the origin of AHE, and some experimental evidences seem to support it [7–13]. This Berry phase theory of the intrinsic AHE includes the Karplus and Luttinger theory in it and has also been applied to spin Hall effect phenomena [14–16], one of the key issues in recent spintronics research. Because the Berry phase in the momentum space is dominated by band crossing points, the intrinsic AHE is very sensitive to a Fermi level shift around the band crossing points [10–13]. For example, Fang *et al.* found a good agreement between theory and experiment on $SrRuO_3$ [11]. They analyzed the AHE of $SrRuO_3$ as a function of magnetization which would be regarded as that of Fermi level shift of each spin band. Lee *et al.* reported doping dependence of the AHE in $CuCr_2Se_{4-x}Br_x$ [12]. However, because their experiments suffered from undesired changes in magnetization and transition temperature by shifting the Fermi level and the electronic structure near the Fermi energy is complex, the change of AHE induced by the Fermi level shift was not fully predictable but rather occasional. Namely, the AHE has been *out of control* determined by the accidental details of the band structure and impurity scatterings. In this Letter, we explore the possibility to control the AHE, even change its sign, by designing the material, structure, and doping level. The system we choose is the single-crystalline thin film of $Eu_{1-x}La_xTiO_3$, which has the ideal band structure near the bottom of the conduction band to show the dramatic change of AHE by doping.

$EuTiO_3$ has a cubic perovskite structure and is a band insulator. The Ti is tetravalent ($3d^0$) and the Eu is divalent. These characteristics are analogous to $SrTiO_3$. The Eu site [$4f^7$ ($S = 7/2$)] orders antiferromagnetically at 5.5 K [17,18]. Katsufuji *et al.* reported that electron carriers could be doped into Ti $3d$ states by substituting divalent Eu with trivalent La [19] as in the case for $Sr_{1-x}La_xTiO_3$. They found that $Eu_{0.9}La_{0.1}TiO_3$ is a ferromagnetic metal. The transition temperature is 8 K and the saturation moment is $7\mu_B$ per Eu, which is identical to the full spin moment of Eu^{2+} ($S = 7/2$). Large negative magnetoresistance around the T_C is observed, indicating the exchange coupling between itinerant electrons and localized spins. In the undoped $EuTiO_3$, Eu^{2+} has $4f$ spins ($S = 7/2$) and interaction between Eu $4f$ spins is dominated by the antiferromagnetic superexchange one through the oxygen $2p$ state and the indirect exchange one through the Eu $5d$ state. By La doping, electrons are introduced into the conduction band of the $3d$ t_{2g} states. There t_{2g} electrons work as another magnetic interaction channel between the Eu spins. In the case of a low carrier density system, such as this compound, the interaction may be ferromagnetic through the Ruderman-Kittel-Kasuya-Yoshida (RKKY) interaction. This system is quite a unique spin-polarized metal in which the carrier density can be tuned with keeping the magnetization constant because Eu spins mainly contribute to the ferromagnetic moment and Ti $3d$ electrons to the metallic conduction. Such properties are suitable for investigating the AHE issued above.

Based on a Luttinger-type effective model [20], we have theoretically examined the relation between the intrinsic contribution of AHE and the band crossings near the conduction band edge. The octahedral crystal field makes the Ti $3d$ orbitals split into e_g ($x^2 - y^2$, $3z^2 - r^2$) and t_{2g} (xy, yz, zx) levels with an energy separation of the order of 1–2 eV, and the top of the oxygen $2p$ valence band is about 3 eV lower than the bottom of the t_{2g} conduction band [21]. Thus it is a good approximation to construct the model from the t_{2g} orbitals at the Ti sites. The hopping between the t_{2g} orbitals and the oxygen $2p$ orbitals is taken into account as an effective hopping matrix between the t_{2g} orbitals. In the cubic structure, it is represented in the first order approximation by the diagonal matrix, $T = \mathrm{diag}(T_y + T_z, T_z + T_x, T_x + T_y)$, where $T_i = 2t[1 - \cos(k_i a)]$, $\boldsymbol{k}$ the lattice momentum, and a the lattice constant. To take into account the spin-orbit interaction, we first consider the projected angular momentum matrices $\bar{\boldsymbol{l}}$ in t_{2g} space just by extracting the 3×3 part of the original 5×5 matrices $\boldsymbol{l}$. The matrices $\bar{\boldsymbol{l}}$ satisfy the commutation relation $[\bar{l}_i, \bar{l}_j] = -i\epsilon_{ijk}\bar{l}_k$. so we will regard $-\bar{\boldsymbol{l}}$ as the effective angular momentum and $\boldsymbol{j}_{\mathrm{eff}} = -\bar{\boldsymbol{l}} + \boldsymbol{s}$ as the effective total angular momentum, where $\boldsymbol{s}$ is the conventional spin-$\frac{1}{2}$ matrix. For the essential understanding, we will focus on the extreme case where the energy splitting due to the on site spin-orbit interaction $\propto \boldsymbol{l} \cdot \boldsymbol{s}$ is sufficiently larger than the energy splitting due to the symmetry lowering from cubic to tetragonal structure. In this case, we can further simplify the model by projecting it from t_{2g} space to the $j_{\mathrm{eff}} = \frac{3}{2}$ space. Then the hopping matrix is reduced to the following form: $T_{\mathrm{eff}} = \sum_{i=x,y,z} T_i(\frac{1}{4} + \frac{j^2_{\mathrm{eff},i}}{3})$.

Around the Γ point, the above model corresponds to the anisotropic limit of the conventional Luttinger model [20]. However, in general, higher order perturbations restore the isotropy. We count this effect by the following additional hopping matrix which preserves the cubic symmetry, $\delta T_{\mathrm{eff}} = \frac{1}{3}\sum_{i\neq j}^{x,y,z} \delta T_{ij} j_{\mathrm{eff},i} j_{\mathrm{eff},j}$, where $\delta T_{ij} = \delta t \sin k_i a \sin k_j a$. In the limit $\delta t = t$, the model reduces to the isotropic Luttinger model [20] around the Γ point. When the system exhibits substantial magnetization anyhow with or without external magnetic field, the exchange interaction is approximated by the effective Zeeman term. The tetragonal distortion induces the energy splitting between the xy orbital and the yz/zx orbitals $V_{\mathrm{tetra}} = \epsilon_{xy} - \epsilon_{yz/zx}$. This perturbation corresponds to the term $-V_{\mathrm{tetra}}\bar{l}_z^2$ in the effective model. Figure 1 shows the band structure of the Luttinger-type effective model, the longitudinal conductivity σ_{xx}, and the intrinsic anomalous Hall conductivity σ_{xy}. The current flows parallel to the x axis; x axis (y axis) corresponds to [100] (or [010]) of film crystal axis, and z axis to the [001]. We can clearly see that the profile of σ_{xy} as a function of the Fermi level is closely correlated with the band crossing points with sign change. Because the intrinsic σ_{xy} is composed of an integration over the Brillouin zone, it is not unusual that the band crossing point of the [001] direction in momentum space affects the σ_{xy} ([010] direction in real space). There appear resonantly enhanced contributions from a pair of hybridized states around a band crossing point, each of which has a sign opposite of the other. The cancellation of σ_{xy} could be observed as shown in Fig. 1. This is a prominent characteristic of the intrinsic AHE as a topological or geometrical phenomenon via Berry's quantal phase. These theoretical predictions might allow us to experimentally control the AHE of $EuTiO_3$ by doping.

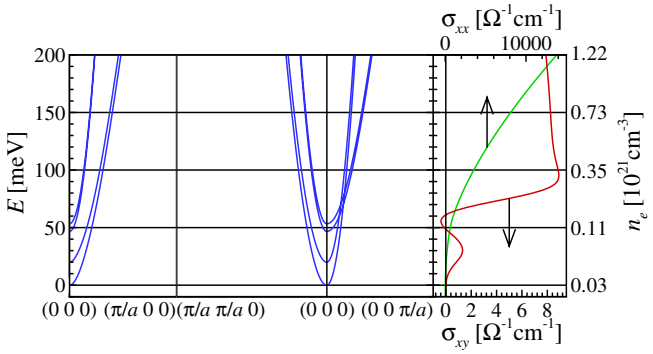

FIG. 1 (color online). Band structure of the Luttinger-type effective model (left-hand panel and middle panel). The right-hand panel shows the Hall conductivity σ_{xy} and the longitudinal (ordinary) conductivity (σ_{xx}) as a function of the Fermi level. Some reference values of the carrier density n_e are indicated on the right vertical axis. The parameters are taken as $t = 300$ meV, $\delta t = -100$ meV, $\Delta_{\mathrm{Zeeman}} = 20$ meV, $V_{\mathrm{tetra}} = 60$ meV, and $a = 4$ Å. The energy broadening is introduced by the constant lifetime τ as $1/\tau = 10$ meV.

Single-crystalline films of $Eu_{1-x}La_xTiO_3$ were fabricated epitaxially on (001) $SrTiO_3$ (STO) and $(LaAlO_3)_{0.3}(Sr_2AlTaO_6)_{0.7}$ (LSAT) single crystal substrates by pulsed laser deposition employing a KrF excimer laser. The laser fluence for the deposition was 1.2 J/cm^2, the repetition rate was 2 Hz, and the substrate temperature was kept at 960 °C in the base pressure (8×10^{-7} Torr). The thickness of all the films was fixed at 10 nm. Thicker films (>30 nm) resulted in the phase mixture of $Eu_{1-x}La_xTiO_3$ and $(Eu_{1-x}La_x)_2Ti_2O_7$ phases. Growth was monitored by reflection high-energy electron diffraction. The intensity of the specular spot was almost constant during the growth because of the step-flow growth mode, which was also confirmed by atomic force microscope image as composed of atomically flat terraces and 4 Å-height steps (perovskite unit cell height). X-ray diffraction measurements indicate that the lattice constant of an $EuTiO_3$/STO(001) film is almost identical with that of bulk $EuTiO_3$ single crystal and free from lattice strain owing to the perfect lattice matching with STO substrate (3.905 Å). On LSAT substrates, due to the larger lattice constant of $EuTiO_3$ (3.905 Å) than that of LSAT (3.868 Å), a tetragonal distortion is epitaxially induced. The in-plane

lattice constant is shortened to match that of LSAT (3.868 Å), while the out-of-plane lattice constant is elongated to 3.940 Å due to the compressive strain. Such lattice distortion from cubic to tetragonal structure changes the crystal field and splits the t_{2g} band degeneracy which should modify the band crossing points. Because the extremely reduced condition is necessary for the deposition of $Eu_{1-x}La_xTiO_3$ as mentioned above, the STO substrate, turned into black, suffers from metallic conduction after the deposition. Therefore, transport properties of the films cannot be evaluated for $Eu_{1-x}La_xTiO_3$/STO(001) films. For magnetization measurement, by contrast, some impurities in LSAT substrate show a Curie-Weiss behavior and disturb the measurement of film magnetic moment itself. Because of such experimental limitations, the magnetization was measured for films on STO(001) while it was measured on the transport property for those on LSAT(001).

Figure 2 shows the temperature dependence of magnetization for a $EuTiO_3$/STO(001) film during warming in a magnetic field of 500 Oe. The arrow at 4 K indicates the kink structure corresponding to a magnetic transition. This transition temperature is almost identical with the antiferromagnetic transition temperature of $EuTiO_3$ bulk crystal [17–19]. The inset shows the magnetic field dependence of magnetization at 2 K. Magnetic field was applied along in-plane [100] (red line) and out-of-plane [001] axes (blue line). The saturation magnetization at a field higher than 0.8 T along the in-plane axis and 2 T along the out-of-plane axis is $7\mu_B$/Eu, which coincides with the full spin moment of Eu^{2+} ($S = 7/2$). Such magnetic anisotropy is caused by the demagnetizing field effect of thin film structure. The kink structure in M-T curve and no remanent magnetization at 2 K in M-H curves shown in Fig. 2 indicate the antiferromagnetic order at the ground state. Such a behavior as magnetic-field induced antiferromagnetic-to-ferromagnetic spin order was previously reported also for bulk crystals [17,19].

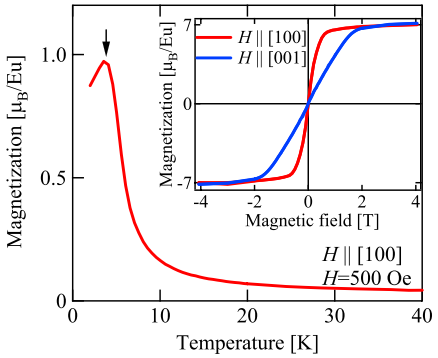

FIG. 2 (color online). Temperature dependence of magnetization at 500 Oe for a $EuTiO_3$/STO(001) film. Inset: Magnetization curves for the film at 2 K. The magnetic field is applied parallel to in-plane [100] (red line) and out-of-plane [001] (blue) axes.

Figure 3 shows the temperature dependence of (a) resistivity and (b) carrier density for $Eu_{1-x}La_xTiO_3$ films on LSAT(001) as well as (c) resistivity for $x = 0.06$ film below 80 K under 0 and 7 T. The current flows parallel to the in-plane [100] (or [010]) axis and the magnetic field is applied parallel to the out-of-plane [001] axis, i.e., the same configuration as the theoretical calculation described above. As shown in the inset of Fig. 3(a), undoped $EuTiO_3$/LSAT(001) film is well insulating. Only 1% La substitution into Eu sites ($x = 0.01$) induces the insulator-to-metal transition, and the resistivity further decreases as x increases. The carrier density was deduced by measurements of Hall effect. The negative sign of the Hall coefficient indicates electrons as charge carriers for all the doped films, which is consistent with the contribution of Ti 3d electron carriers. As shown in Fig. 3(b), the carrier density systematically increases as x increases. The ratio between the activated carrier density and the doped La density is between 50% and 100%, severely affected by the crystalline quality of films; the carrier density does not linearly increase from $x = 0.01$ to 0.06. A similar behavior was also reported in $Sr_{1-x}La_xTiO_3$ films [22]. As shown in Fig. 3(c), a kink structure is obviously seen at 8 K and large negative magnetoresistance is observed under 7 T. The origin of this kink structure should be the magnetic

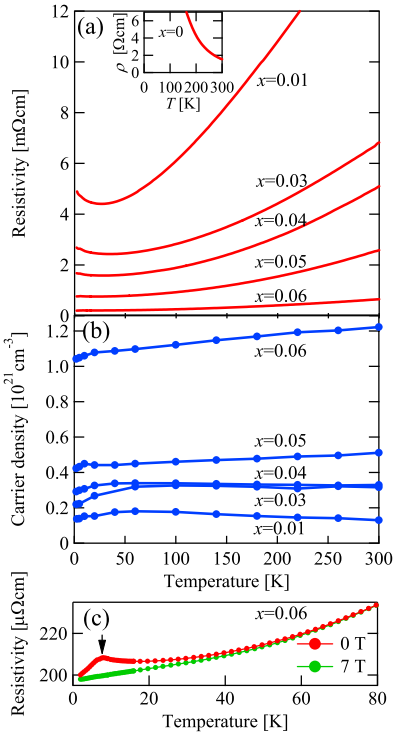

FIG. 3 (color online). Temperature dependence of (a) resistivity and (b) carrier density for $Eu_{1-x}La_xTiO_3$/LSAT(001) films from $x = 0.01$ to 0.06. Inset of (a) shows the data for a pristine $EuTiO_3$/LSAT(001) film. (c) Temperature dependence of resistivity for a $Eu_{0.94}La_{0.06}TiO_3$/LSAT(001) film under 0 and 7 T below 80 K. The arrow indicates a magnetic transition at 8 K.

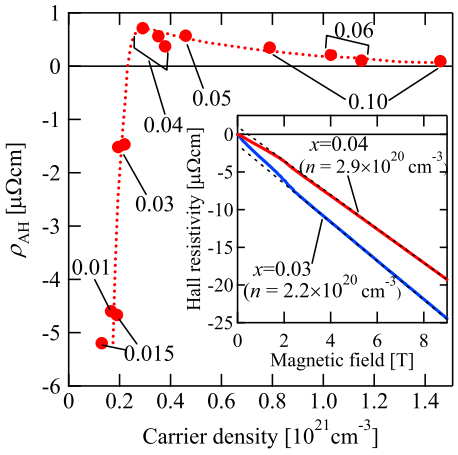

FIG. 4 (color online). Carrier density dependence of anomalous Hall resistivity (ρ_{AH}) for $Eu_{1-x}La_xTiO_3$/LSAT(001) films at 2 K. The number for each data point is the nominal electron concentration x and the dotted curve is a guide to the eyes. The inset shows the magnetic field dependence of Hall resistivity for $Eu_{1-x}La_xTiO_3$/LSAT(001) films with $x = 0.03$ and $x = 0.04$ at 2 K.

transition as observed in the temperature dependence of magnetization for undoped $EuTiO_3$/STO(001) in Fig. 2. The transition temperature gradually increases from 5 to 8 K as the La concentration increases. Such behaviors of transport imply the exchange coupling between Eu spins and Ti 3d carrier electrons. Because of the coupling, the Ti 3d electrons are spin polarized when Eu spins are ferromagnetically aligned by an external magnetic field, showing the negative magnetoresistance around the transition temperature; this is characteristic of ferromagnetic metals.

The AHE for $Eu_{1-x}La_xTiO_3$/LSAT(001) films was measured at 2 K. The inset of Fig. 4 shows the typical magnetic field dependence of Hall resistivity for $x = 0.03$ and 0.04 films. The anomalous Hall resistivity (ρ_{AH}) was determined by the extrapolation of the field-linear part as indicated by dotted lines. The linear part corresponds to the normal Hall effect term and is used also for deriving the carrier density. The deviations from the linear part occur below 2 T. This magnetic field almost coincides with the saturation field of magnetization as shown in the inset of Fig. 2 ($H \parallel c$). The main panel of Fig. 4 shows the ρ_{AH} as a function of carrier density. The denotation numbers represent the x and the dotted curve is a guide to the eyes. Interestingly, the ρ_{AH} does not show a monotonic dependence, but the sign changes from negative to positive as the carrier density increases. The sign change occurs between $n = 2.2 \times 10^{20}$ cm^{-3} and 2.9×10^{20} cm^{-3}, that can also be clearly discerned from the raw data shown in the inset of Fig. 4. Note that a band conduction is dominant in this carrier density (band filling) range although a tiny upturn can be seen in the temperature dependence of resistivity [Fig. 3(a)]. Thus, the origin of the AHE in this compound is not extrinsic but intrinsic; the carrier density dependence of ρ_{AH}, including the sign change, should be related to the band structure of t_{2g} conduction bands. ρ_{AH} is expressed as $\rho_{AH} = \frac{\sigma_{xy}}{\sigma_{xx}^2 + \sigma_{xy}^2}$. The orders of magnitude for σ_{xy} ($\sim 1\ \Omega^{-1}\,\mathrm{cm}^{-1}$) is rather small compared to regular ferromagnetic metals, e.g., bcc Fe ($\sim 700\ \Omega^{-1}\,\mathrm{cm}^{-1}$), because the larger broadening due to the disorder scattering, which can be roughly estimated from σ_{xx}^{-1}, makes the resonant contribution to the intrinsic anomalous Hall conductivity σ_{xy} smaller. Qualitatively, the sign change as observed in Fig. 4 seems to correspond to the behavior of σ_{xy} around $E = 60$ meV in Fig. 1, indicating the correlation between the sign change of ρ_{AH} and the band crossing points. Although the quantitative understanding requires a more exact treatment than that based on the effective model, the Fermi level shift by doping certainly varies ρ_{AH} as the model calculation predicted.

In summary, we have demonstrated the control of the AHE in electron doped $EuTiO_3$ by fabricating epitaxial $Eu_{1-x}La_xTiO_3$ films. The AHE can be controlled by the doping concentration x of the spin-polarized carriers. It was found that the anomalous Hall resistivity varies significantly as a function of the carrier density, while the sign changes at around $n = 2.4 \times 10^{20}$ cm^{-3}. These results for the electron doped $EuTiO_3$ film prove the AHE as controllable values by designing a model compound with the simple band structure near $\boldsymbol{k} = 0$.

[1] S. A. Wolf *et al.*, Science **294**, 1488 (2001).
[2] I. Žutić *et al.*, Rev. Mod. Phys. **76**, 323 (2004).
[3] *Concepts in Spin Electronics*, edited by S. Maekawa (Oxford University, London, 2006).
[4] R. Karplus and J. M. Luttinger, Phys. Rev. **95**, 1154 (1954).
[5] J. Smit, Physica (Amsterdam) **24**, 39 (1958).
[6] L. Berger, Phys. Rev. B **2**, 4559 (1970).
[7] J. Ye *et al.*, Phys. Rev. Lett. **83**, 3737 (1999).
[8] S. H. Chun *et al.*, Phys. Rev. Lett. **84**, 757 (2000).
[9] T. Jungwirth *et al.*, Phys. Rev. Lett. **88**, 207208 (2002).
[10] M. Onoda and N. Nagaosa, J. Phys. Soc. Jpn. **71**, 19 (2002).
[11] Z. Fang *et al.*, Science **302**, 92 (2003).
[12] W.-L. Lee *et al.*, Science **303**, 1647 (2004).
[13] Y. Yao *et al.*, Phys. Rev. Lett. **92**, 037204 (2004).
[14] S. Murakami *et al.*, Science **301**, 1348 (2003).
[15] Y. K. Kato *et al.*, Science **306**, 1910 (2004).
[16] J. Wunderlich *et al.*, Phys. Rev. Lett. **94**, 047204 (2005).
[17] T. R. McGuire *et al.*, J. Appl. Phys. **37**, 981 (1966).
[18] C.-L. Chien *et al.*, Phys. Rev. B **10**, 3913 (1974).
[19] T. Katsufuji and Y. Tokura, Phys. Rev. B **60**, R15 021 (1999).
[20] J. M. Luttinger, Phys. Rev. **102**, 1030 (1956).
[21] R. Ranjan *et al.*, J. Phys. Condens. Matter **19**, 406217 (2007).
[22] D. Olaya *et al.*, Appl. Phys. Lett. **80**, 2928 (2002).